Energetic Comparison of Linear Fresnel and Parabolic Trough Collector Systems

Heiko Schenk
German Aerospace Center (DLR),
Institute of Solar Research,
Wankelstraße 5,
Stuttgart 70563, Germany
e-mail: Heiko.Schenk@dlr.de

Tobias Hirsch
German Aerospace Center (DLR),
Institute of Solar Research,
Wankelstraße 5,
Stuttgart 70563, Germany
e-mail: Tobias.Hirsch@dlr.de

Jan Fabian Feldhoff
German Aerospace Center (DLR),
Institute of Solar Research,
Wankelstraße 5,
Stuttgart 70563, Germany
e-mail: Jan.Feldhoff@dlr.de

Michael Wittmann
German Aerospace Center (DLR),
Institute of Solar Research,
Wankelstraße 5,
Stuttgart 70563, Germany
e-mail: Michael.Wittmann@dlr.de

*In recent years, linear Fresnel (LF) collector systems have been developed as a technical alternative to parabolic trough (PT) collector systems. While in the past, LF systems focused on low- and medium-temperature applications, today, LF systems are equipped with vacuum receivers and, therefore, can be operated with similar operating parameters as PT systems. Papers about the technical and economical comparison of specific PT and LF systems have already been published (Dersch et al., 2009, "Comparison of Linear Fresnel and Parabolic Trough Collecor Systems—System Analysis to Determine Break-Even Costs of Linear Fresnel Collectors," Proceedings of the 15th International SolarPACES Symposium, Berlin; Giostri et al. 2011, "Comparison of Two Linear Collectors in Solar Thermal Plants: Parabolic Trough vs. Fresnel," ASME 2011 5th International Conference on Energy Sustainability, Washington, DC; and Morin et al., 2012, "Comparison of Linear Fresnel and Parabolic Trough Collector Power Plants," Sol. Energy, **86**(1), pp. 1–12). However, the present paper focuses on the systematic differences in optical and thermodynamic performance and the impact on the economic figures. In a first step the optical performance of typical PT and LF solar fields (SFs) has been examined, showing the differences during the course of the day and annually. Furthermore, the thermodynamic performance, depending on the operating temperature, has been compared. In a second step, the annual electricity yield of typical PT and LF plants has been examined. Solar Salt has been chosen as the heat transfer fluid. Both systems utilize the same power block (PB) and storage type. Solar field size, storage capacity, and PB electrical power are variable, while all examined configurations achieve the same annual electricity yield. As expected for molten salt systems, both systems are the most cost-effective with large storage capacities. The lower thermodynamic performance of the LF system requires a larger SF and lower specific SF costs in order to be competitive. Assuming specific PT field costs of 300 €/m^2 aperture, the break-even costs of the LF system with Solar Salt range between 202 and 235 €/m^2, depending on the site and storage capacity. In order to confirm the major statements, within a sensitivity analysis, it is shown that a variation of SF and storage costs does not have a significant impact on the relative break-even costs of the LF system.* [DOI: 10.1115/1.4027766]

Keywords: linear Fresnel, parabolic trough, system comparison, solar thermal power plant, thermal energy storage, solar field cost, molten salt

1 Introduction

Driven by the increasing activities in CSP technology within the last years, LF collector systems have been developed as a technical alternative to PT collector systems. While LF have been designed for lower temperature applications in the past, recent developments show that both line-focusing collector systems can, in principle, be used for the same thermodynamic processes. Nevertheless, the different characteristics, especially optical performance, have to be considered in the design of a complete system. Although some studies about comparison of PT and LF applications have been published [1–3], a study focusing on the systematic differences in energetic performance has not been conducted. It is the intention of this paper to provide a methodology for a systematic comparison and first results comparing PT and LF systems. Thus, in a first step, the applied methodology is described. In a second step, the systematic differences between the two concepts are worked out.

Contributed by the Solar Energy Division of ASME for publication in the Journal of Solar Energy Engineering. Manuscript received May 24, 2013; final manuscript received May 22, 2014; published online June 20, 2014. Assoc. Editor: Wojciech Lipinski.

2 Methodology

The intention of the paper is to provide a systematic comparison of PT and LF systems. Thus, we concentrate on keeping boundary conditions similar for both systems wherever possible. A stepwise analysis along the efficiency chain reveals the major differences between both systems and their impact for representative applications. At some points, we introduce simplifications to make both systems comparable. We are aware that, after an optimization of the plant, the layout and thermodynamic parameters might be slightly different from the layouts we choose for this comparison. However, the resulting deviations are considered to be small compared to the major differences between the two collector systems.

Furthermore, we follow the approach that both systems should by default deliver the same amount of energy per year. By varying SF size, PB capacity, and storage capacity we identify a number of configurations that result in the same annual yield. Based on these thermodynamic calculations, a cost study is presented. In this study, the evolution of break-even costs of the LF system depending on storage and PB capacity is shown. Recent tests results from PT as well as LF show that both systems are able to operate in the same temperature range. Thus, for the system

comparison the same fluid cycle is assumed for both systems. The remaining difference is in the collector performance, namely, the optical performance.

3 Definitions

Since PT and LF are both line-focusing systems, their heat balance can be described with the same set of equations. The current optical efficiency of the SF can be calculated as follows:

$$\eta_{\text{opt}} = \eta_{\text{opt},0} \cdot \text{IAM} \cdot \eta_{\text{shad}} \cdot \eta_{\text{end}} \cdot \eta_{\text{clean}} \tag{1}$$

where $\eta_{\text{opt},0}$ describes the maximal optical efficiency at perpendicular incidence of sun rays on a perfectly clean mirror which is not shaded. The efficiency is by definition related to the net aperture area A_{net}, which represents the effective projected aperture area of the collector excluding gaps between mirrors. The incidence angle modifier (IAM) describes the reduction of the optical efficiency, in case of the PT system due to the incidence angle, and in case of the LF system due to the incidence angle and the transversal angle. The factor η_{clean} describes the reduction of the optical efficiency due to soiling of mirrors. When the incidence angle is flat, in PT and in LF systems, optical end losses occur since at the collectors' ends a fraction of the reflected solar irradiation does not impinge on the receiver. Those losses are accounted for by the factor η_{end} (for a definition see Ref. [3]). Furthermore, in parallel, PT collector rows' shading occurs when the sun's elevation is low (for a definition also see Ref. [3]). Shading in parallel LF rows, usually, either is neglected or integrated in the IAM function.

The effective specific optical input to the SF is calculated with Eq. (2) and the optical power with Eq. (3).

$$\dot{q}_{\text{solar}} = \text{DNI} \cdot \eta_{\text{opt}} \tag{2}$$

$$\dot{Q}_{\text{solar}} = \dot{q}_{\text{solar}} \cdot A_{\text{net}} \tag{3}$$

In order to calculate the current thermal efficiency of the SF the effective current thermal power is related to the available optical power:

$$\eta_{\text{therm,SF}} = \frac{\dot{Q}_{\text{solar}} - \dot{Q}_{\text{loss,col}} - \dot{Q}_{\text{loss,H\&P}}}{\text{DNI} \cdot A_{\text{net}}} \tag{4}$$

where $\dot{Q}_{\text{loss,col}}$ represents the heat losses of the receivers in all collectors and $\dot{Q}_{\text{loss,H\&P}}$ the heat losses of all other pipes and equipment in the SF. The numerator of the fraction represents the effective thermal power of the SF and can be described as $\dot{Q}_{\text{SF}}$.

In order to characterize the layout of CSP power plants, the solar multiple (SM) is often used. The SM describes the degree of oversizing of the SF in relation to the PB:

$$\text{SM} = \frac{\dot{Q}_{\text{SF,nom}}}{\dot{Q}_{\text{PB,nom}}} \tag{5}$$

where $\dot{Q}_{\text{PB,nom}}$ represents the thermal input to the PB at its nominal operation point and $\dot{Q}_{\text{SF,nom}}$ the thermal SF power at nominal irradiation conditions. These nominal conditions are arbitrary. However, usually a direct normal irradiance (DNI) of 800–900 W/m^2 at perpendicular irradiation and perfectly clean mirrors is chosen.

For example, while the SM of PT plants without thermal energy storage (TES) ranges between 1 and 1.4, plants with a significant storage capacity need an oversized SF in order to be able to charge the TES system. For example, the SM of a PT plant with a storage capacity of eight full-load hours tends to range between 1.6 and 2. Note that this range of SM is given in Ref. [4] for the plants using synthetic oil as the heat transfer fluid. The cost structure of plants with molten salt as heat transfer fluid could shift these optima.

4 Reference Systems

4.1 Thermodynamic Cycle. A number of different heat transfer fluids are discussed for the application in line-focusing plants. The state-of-the-art for PT is synthetic oil which limits operation temperatures to about 400 °C. Direct steam generation (DSG) PT systems are ready to enter the market and a first commercial plant with steam parameters of 35 bar/340 °C has gone into operation in Thailand by the end of 2011 [5]. DLR demonstrated collector operation at 500 °C in a Spanish test facility [6].

First LF plants have been built in Spain by Novatec Solar with a saturated steam process at 55 bar [7]. The same company successfully tested its collector system for process temperatures up to 500 °C, using a vacuum receiver tube similar to the one applied in PT [8]. From today's viewpoint, both, the PT and LF system, are ready to be operated up to high process temperatures. In order to make use of the inherent advantages of concentrating solar thermal power plants compared to photovoltaic electricity generation, the systems in focus are equipped with TES systems. Although a number of technical challenges have to be solved, a molten salt cycle was chosen for the present study:

- A technical solution for large storage capacities with a direct two-tank storage system is available.
- Due to the direct storage system, there is no major difference between SF and storage operation points (compared to oil-based systems where in storage mode the PB is operated at reduced temperature and load).
- High temperatures around 500 °C or more can be reached.
- Single-phase heat transfer fluid simplifies the system comparison.

4.2 Parabolic Trough Reference System. The first solar electricity generating system (SEGS) plants in the United States were equipped with LS-1 collectors with an aperture width of 2.55 m. Due to the better focusing capability with the successor modes LS-2 and LS-3 higher concentration factors could be attained by increasing the aperture width overproportionally compared to the receiver diameter. Both collector types have also been installed in the SEGS plants. The aperture width of 5.76 m of the LS-3 collector developed into a standard for PT collectors of the current generation. For the Spanish market, a new collector system, the SKAL-ET (scaled Eurotrough) was developed. By increasing the length (SKAL-ET: 150 m, LS3: 100 m) and by modifying the collector structure further cost reduction was achieved. With the ultimate trough a new generation of trough collectors with an again larger aperture width was announced. However, the ultimate trough has not been realized in commercial projects, yet [9]. A comprehensive review on different collectors is available from Ref. [10].

The optical performance of trough collectors, which are in operation in Spain, today, is very similar. Thus, this paper refers to a SKAL-ET class collector since performance data are publically available [11]. The incidence-angle-dependent optical performance of the collector is expressed with the IAM and is very similar for most of the PT collectors. The IAM of the SKAL-ET, in which cosine losses already are included, is plotted in Fig. 1.

Today, collector manufacturers make use of commercially available receivers. For the present study Schott's PTR 70 is chosen as Ref. [12]. Whereas the commercial version allows operating temperatures up to 450 °C, [13], in the REAL-DISS project, a modified version of the receiver was adapted to operating temperatures up to 500 °C [6].

Relevant performance parameters are shown in Table 1. At nominal conditions (850 W/m^2 at perpendicular incidence, 500 °C) an optical input per unit length of collector of 3.3 kW/m is attained. The collector field shall have a similar shape as in state-of-the-art oil-based plants, where a loop consists of four collectors with a total receiver length of 600 m. The collector axis shall be aligned in North-South direction.

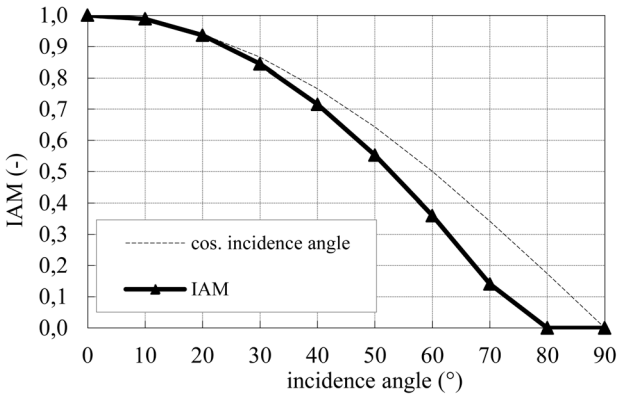

Fig. 1 Cosine of incident angle and IAM of the PT collector

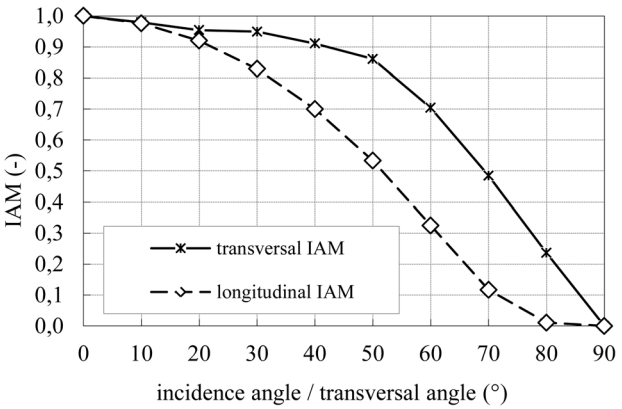

Fig. 2 Longitudinal and transversal IAM of the LF collector

Table 1 Parameters of PT collector and SF

Collector type	SKAL-ET
Aperture width/length	5.8 m/150 m
Net aperture area collector	817.5 m
Number of collectors per loop	4
Focal length	1.71 m
Row distance (center to center)	3 × aperture width = 17.3 m
Orientation	North-South
Peak optical efficiency (related to net aperture area)	78%
Average mirror cleanliness	98%
IAM	See Fig. 1
Outer diameter of absorber tube	70 mm
Receiver type/heat losses of receiver	Schott PTR 70 according to Ref. [12]
Heat transfer fluid	Solar salt

Table 2 Parameters of LF collector and SF

Collector type	SUPERNOVA
Module length/width	44.8 m/16.7 m
Net aperture area of module	513.6 m^2
Number of modules per collector	13
Length of collector	582.4 m
Focal length	7.4 m
Number of collectors per loop	1
Row distance (center to center)	21.5 m
Orientation	North-South
Peak optical efficiency (related to net aperture area)	65%
Average mirror cleanliness	98%
IAM	See Fig. 2
Outer diameter of absorber tube	70 mm
Receiver type/Heat losses of receiver	Schott PTR 70 according to Ref. [12]
Heat transfer fluid	Solar salt

4.3 Linear Fresnel Reference System. There are two LF collector concepts currently being realized in commercial plants. One is by Novatec Solar and the other by Areva solar [14]. Some other concepts have been followed by Solar Power Group [15]. For the technology comparison, we will refer to the so-called SUPERNOVA system by Novatec Solar [8]. This system is based on the Nova 1 collector that already has proven its reliability in the PE-1 and PE-2 plants, Puerto Errado, Spain. Due to the implementation of vacuum receiver tubes superheated steam at up to 500 °C can be produced with the SUPERNOVA system.

In the present study, molten salt as heat transfer fluid is chosen. Since the SF outlet temperature is set to 500 °C, the considered SF entirely consists of the new generation of LF collectors with vacuum receiver. Reliable data for the optical performance of the NOVA-1 collector are publically available [16]. Due to the use of a vacuum receiver, the optical efficiency of the collector decreases by 2% to 3%, [7], while the IAM-characteristics remain similar to the ones of the NOVA-1 collector. The IAM is expressed as a product of a transversal and a longitudinal component according to [16]:

$$\mathrm{IAM} = \mathrm{IAM}_{\mathrm{trans}}(\theta_{\mathrm{trans}}) \times \mathrm{IAM}_{\mathrm{long}}(\theta_{\mathrm{i}}) \tag{6}$$

where θ_{trans} represents the transversal angle and θ_{I} the incidence angle. The result of Eq. (6) is plotted in Fig. 2. A definition of angles can be found in Ref. [3].

In Table 2, the collector and SF parameters, which are considered in the present study, are summarized. At nominal conditions (850 W/m^2 at perpendicular irradiation, 500 °C), an optical input of 6 kW/m is attained, which is higher than that of the PT system.

Table 3 Metrological data of Daggett and Seville

	Unit	Daggett (CA)	Seville (Spain)
Latitude/longitude	(deg)	34.85/–116.8	37.4/–5.98
Annual DNI sum	(kWh/m^2)	2724	1881
Mean/min/max. temperature	(°C)	16.3/–5.0/46.7	18.3/2.3/40.5

4.4 Further Technical and Site Data. Two reference sites have been chosen: Daggett, California, United States, and Seville, Spain. Irradiation data for Daggett are publically availably [17] whereas the data for Seville have been generated with the commercial software METEONORM [18]. Characteristic data for both sites are shown in Table 3.

The SFs of PT and LF systems have already been described in Secs. 4.2 and 4.3. All further important plant parameters can be found in Table 4. As heat transfer fluid in the SF and in the sensible two-tank storage system solar salt (60% $NaCO_3$, 40% KNO_3) is chosen since it represents the commercial molten salt solution until today. The utilization of molten salt in PTs, as well as the thermophysical properties is discussed in Ref. [19]. The minimal salt temperature in the plant is set to 260 °C in order to avoid solidification. For both systems the nominal operating point is set to a DNI of 850 W/m^2 (perpendicular incidence), which serves as reference for the SM (see Eq. (5)).

The losses of the headers and piping $\dot{Q}_{\mathrm{loss,H\&P}}$ of the SF occur at nominal operating temperature. In the present study, we assume that the heat losses of PT system are about twice as high as the

Table 4 Plant specifications

	Unit	PT	LF
Nominal DNI at perpendicular incidence	(W/m^2)	850	
Nominal T_{amb}	(°C)	20	
Specific heat loss of SF headers and piping related to A_{net} ($\dot{Q}_{loss,H\&P}$)	(W/m^2)	15	7.5
SF inlet/outlet temperature	(°C)	290/500	
Heat transfer medium		Solar salt	
Antifreeze temperature	(°C)	260	
Land use factor (related to A_{net})	(-)	3.5	2
Solar multiple SM		1.2…3	
PB gross efficiency	(%)	42	
PB nominal gross power	(MW)	20…100	
Minimum, maximum thermal PB load	(%)	15/102	
Storage type		Direct two tank solar salt	
Temperatures of hot/cold storage tank	(°C)	500/290	
Storage capacity C_{TES}	(FLH)	2,4,6,8,10,12,14	
Max. annual fossil cofiring	(%)	15 (as in Spain)	

ones of the LF system. This is due to the fact that the LF system consists of a smaller number of loops, and furthermore, no flexible pipe connections are necessary (as in the PT system).

The size of the SF, the gross electrical power of the PB and the number of full load hours (FLH) of the TES will be varied (see Sec. 7). Note that the storage capacity is related to the number of FLH of the PB. Hence, solutions with constant storage capacity in FLH do not have the same capacity in MW h. In molten salt plants, the storage system tends to be less expensive and more efficient than in thermal oil plants, since no heat-exchangers are necessary. Hence, molten salt plants without TES tend to be less economical but, for the sake of completeness, they are also considered in the present study.

Wet cooling conditions are assumed for the PB and its gross efficiency is set to 42%. This value has been determined in an internal analysis for a plant operating temperature of 500 °C. The gross efficiency of the PB in PT plants with thermal oil, that operate at 390 °C the efficiency can be up to 40%, see Ref. [20] and for molten salt towers with higher temperatures (565 °C), efficiencies of 43% are announced [21]. Both examples confirm the chosen value of 42% as realistic. The allowed cofiring is defined as the fuel equivalent that is necessary to produce 15% of the generated electricity of the plant.

5 Optical Performance

In the first step, we compare the optical efficiency of the PT and LF systems. There is an inherent difference between the peak optical efficiency which is higher for the PT system (see Secs. 4.2 and 4.3).

The tracking angle ρ_{tr} of the PT system corresponds to the transversal angle of the LF system ($\theta_{trans,.LF} = \rho_{tr,PT}$). While the optical performance of a PT field is only affected by high tracking angles (which correspond to very low sun heights—see curve for $\rho_{tr} = 80$ deg in Fig. 3) due to shading between collector rows, the optical performance of a LF system strongly depends on the transversal angle θ_{trans}. The reason is that the primary reflectors of the LF have to be designed for a certain transversal angle. For all other transversal angles, the curvature of the mirror panels is not optimal. Additionally, blocking and shading between mirror facets occurs. In contrast, the parabolic shape of the PT mirror surface is the optimum reflecting surface independent of the track angle. However, optical end losses occur in PT as well as in LF field.

Figure 3 shows the optical efficiency of a PT and a LF field over the incidence angle θ_i for different transversal angles θ_{trans} (or ρ_{tr}, respectively). From here, it becomes clear that the optical performance of the PT system is systematically better than the one of the LF system, especially for high transversal angles.

Figures 4 and 5 show the sorted distribution of the DNI, the IAM-corrected DNI, and the specific optical input, $\dot{q}_{solar}$ for both sites. By comparing both sites it becomes clear that the maximal DNI in Daggett is higher than the one in Seville, and also there are more annual hours with direct solar irradiation. By observing the curves for $\dot{q}_{solar}$, there is a significant offset between the LF and the PT system, which is due to the lower optical efficiency.

The curve of the IAM-corrected DNI shows that the LF system is already penalized by its IAM-characteristics. Hence, by oversizing a Fresnel field similar nominal optical power can be attained, but the IAM-characteristics would still lead to more operation hours in part-load and to probably less operating hours per year.

As representative examples the optical performance of the PT and LF systems are evaluated for three clear-sky days, one typical

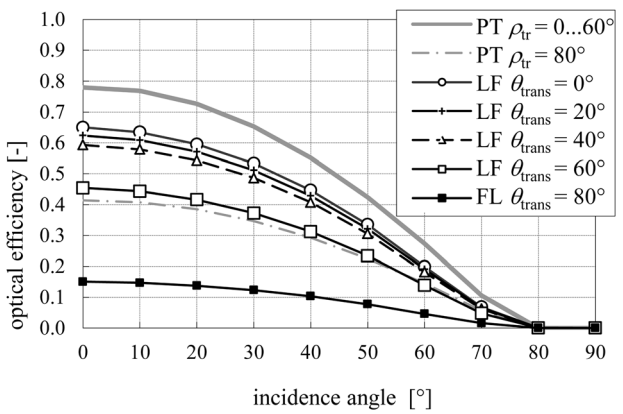

Fig. 3 Optical efficiency of PT and LF system including field losses (shading and end losses)

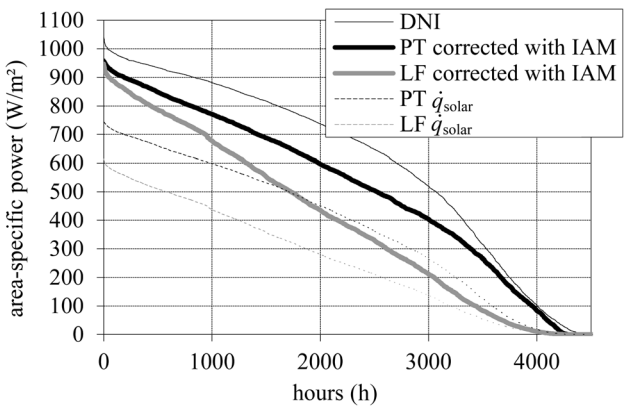

Fig. 4 Annual distribution of DNI, IAM-corrected DNI, and area-specific optical input for Daggett

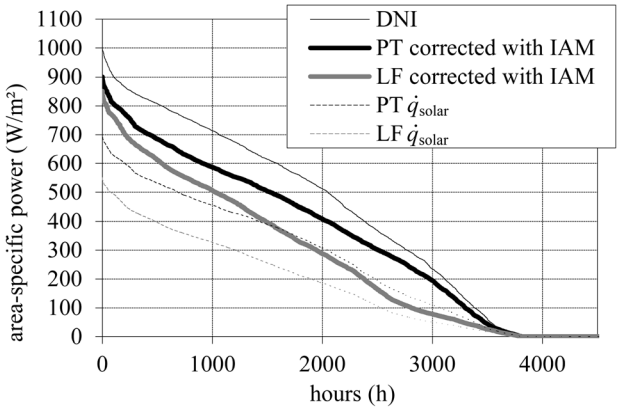

Fig. 5 Annual distribution of DNI, IAM-corrected DNI, and area-specific optical input for Seville

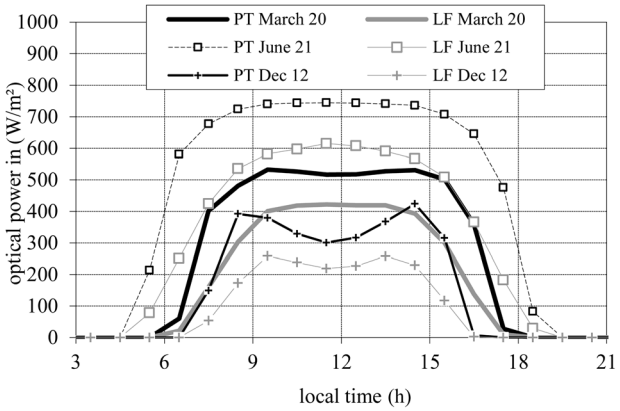

Fig. 7 Optical power ($\dot{q}_{solar}$) of a PT and LF system on Mar. 20, June 21, and Dec. 12 for Daggett

winter day close to winter solstice, 1 day close to equinox, and 1 day in the summer season in Daggett (Dec. 12, Mar. 20, and Jun. 21). Figure 6 shows the DNI and the elevation of the sun α_s. As visible, the maximal DNI on a clear-sky winter day (Dec. 12) can be as high as in summer and higher than on the day in March at this site. However, the energy yield of both systems, PT and LF, will be lower in winter than in summer due to two phenomena:

- The duration of the day is shorter.
- The lower sun elevation α_s leads to greater incidence angles for both systems and to greater transversal angles for the LF system, which diminishes the optical performance (compare with Fig. 3).

Figure 7 shows the optical power input $\dot{q}_{solar}$ of both systems. Due to the North-South orientation the optical performance of PT system is higher in the morning and evening than on solar noon. In combination with the daily evolution of the DNI (which attains its maximum at solar noon), a wide plateau of almost constant optical yield is attained. In contrast, the optical performance of the Fresnel system attains its peak at solar noon entailing a mid-day peak of solar power, in summer. On the winter day and the day close to equinox, $\dot{q}_{solar}$ can also be described as a plateau which is, nevertheless, much shorter than the one of the PT system.

For an efficient use of a power cycle the PT system is in favor, since the number of part-load operating hours is smaller. For a LF system, the PB must either be designed larger or a significant amount of thermal energy must be dumped during the overload periods. Furthermore, independently from the dimensions of the SF, the operating period with relevant output is shorter for the LF system.

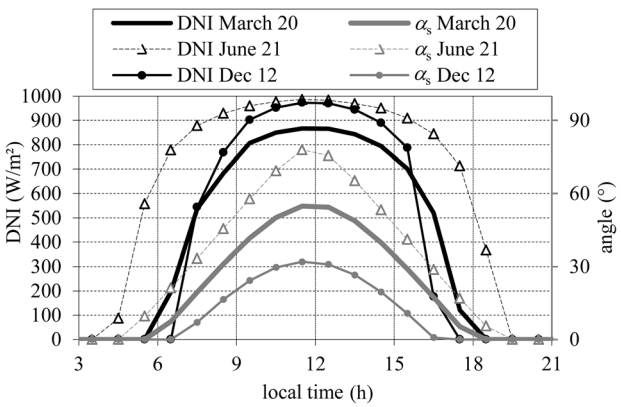

Fig. 6 DNI and sun elevation α_s Mar. 20, June 21, and Dec. 12 for Daggett

6 Thermal Performance

While the optical performance is the main difference between PT and LF, the heat loss characteristics are quite similar since the same receivers are installed. Nevertheless, in the Fresnel system there are less running meters of receiver tubes, and furthermore, the specific heat losses of headers and piping are lower (compare with Sec. 4.4). Hence, the area-specific heat losses (receivers and piping together) are lower in the LF system than in the PT system, see Fig. 8. Figure 9 shows the thermal efficiency $\eta_{therm,field}$ (Eq. (4), Sec. 3) of both systems for two different DNI (perpendicular irradiation) over the difference between ambient and fluid temperature. Although the heat losses of the Fresnel system are lower, they cannot compensate for the inferior optical performance. Nevertheless, the differences in curvatures indicate that the Fresnel system is more tolerant toward higher process temperature.

7 Plant Performance

7.1 Description of Thermodynamic Plant Model. The thermodynamic results of the present study have been generated with a DLR-internal thermodynamic model. The model initially was developed for the Ecostar-study [22]. The model is able to calculate annual energy yields of line-focusing CSP plants with typical heat transfer fluids such as thermal oil, water/steam, and molten salt. While originally the model was steady-state-based, thermal masses are now considered in order to represent start-up and cool-down procedures.

A simple solar-driven operating strategy is implemented. After sunset, the PB is operated in full load until the TES is discharged.

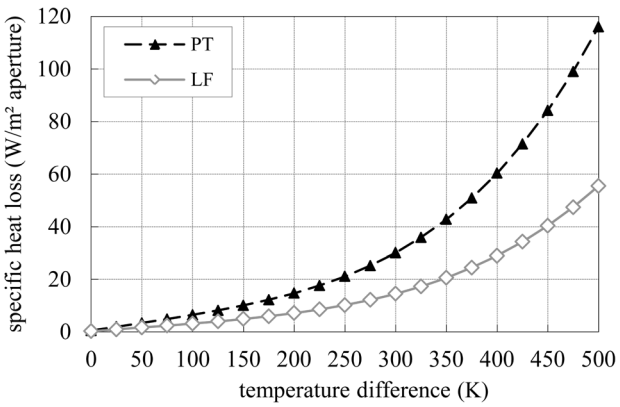

Fig. 8 Specific heat losses of the collector systems

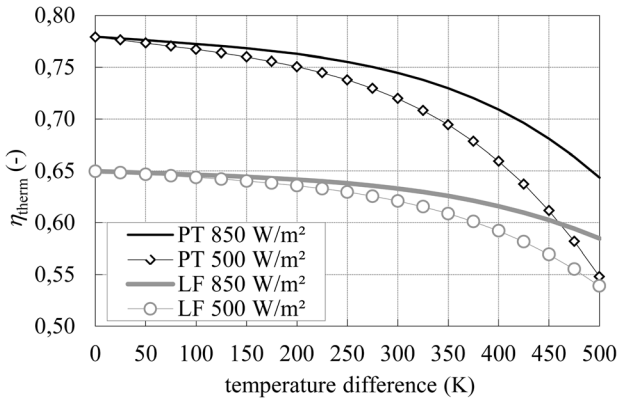

Fig. 9 Thermal efficiency of collector field at DNI = 850 W/m² and 500 W/m² (perpendicular irradiation)

When the SF attains its minimal temperature, antifreeze operation is provided by fossil cofiring. The remaining allowed annual cofing energy (15% in this case) is used to produce electricity.

7.2 Assumptions. The analysis of the plant performance requires the definition of some more boundary conditions. The general approach is to compare configurations that generate the same annual net electrical output W_{net}. Furthermore, systems with a wide range of storage capacities (0…14 FLH) shall be considered. Having the thermodynamic process parameters fixed, the plant layout is defined by three major design values:

- SF size $A_{net,SF}$ (m^2)
- nominal gross power of the PB $P_{el,gross}$ (MW)
- storage capacity C_{TES} (FLH)

The SM is derived from A_{net} and C_{TES}. Having in mind the differences in the daily output of PT and LF it would not be fair to compare systems with the same annual output and at the same time define the same PB capacity for both systems. In fact for a LF system, the optimum PB capacity might be different from the one of the PT system. One further major assumption is to consider the efficiency of the three main components (SF, PB, and TES) unaffected by their size. For example, this means that the nominal gross efficiency of the smallest PB in the study, 37 MW, equals the nominal gross efficiency of the largest PB, 110 MW. In fact, the nominal efficiency of PBs of this range change rather marginally. However, in a more detailed case study with specific systems, the differing nominal efficiency of each PB should be considered.

With the above-mentioned assumptions the component sizes can be related relative to each other in terms of:

- SM
- FLH of the TES system

In that manner, we can compare PT and LF configurations with various combinations of SF size, PB electrical power and storage capacity whose annual electricity yield is equal. In a second step, an economic optimization is carried out in order to find the cost-optimized configurations for each category of storage capacity.

7.3 Economic Analysis. Since the thermodynamic process is the same for both systems we can assume the same specific investment costs (CI) for PB and storage system. The significant difference is in the specific SF costs which are announced to be significantly lower for the LF than for the PT system (if related to aperture area). In contrast to previous publications [1,3] the present paper avoids comparing PT and LF systems in terms of levelized cost of electricity. In order to do so, the following assumptions are made:

Table 5 Financial parameters

	unit	PT	LF
Specific cost of SF	(€/m^2)	300	200…250
Specific cost of PB	(€/kW_{el})		700
Specific cost of TES	(€/kW h_{th})		30
Specific cost of land	(€/m^2)		8
Surcharges for construction	(%)		20

- The operation and maintenance (O&M) costs of both systems are equal.
- Due to different operating times of the set of presented solutions, the offline parasitics might slightly differ. However, this difference is neglected.
- The price of sold electricity is not variable (constant feed-in tariff); hence, the daily repartition of W_{net} does not have an economic impact.

Since all examined solutions provide the same W_{net} they can be compared by their CI. From the CI the break-even costs $c_{SF,b\text{-}e}$ of the LF field can be deduced for various storage capacities and for the two sites Daggett and Seville. $c_{SF,b\text{-}e}$ represent the highest specific cost of SF of the LF system at which competitiveness with a comparable PT system is achieved.

As a basis we assume PB costs of 700 €/kW_{el} and storage costs of 30 €/kWh_{th}. The PT field costs are estimated to be 300 €/m^2 related to net aperture area (including foundations, leveling, HTF, and all components). It should be noted that specific costs are assumed to be independent from the plant component size. Furthermore, a surcharge rate for construction of 20% is assumed. These 20% are added to the total equipment costs (which consist of SF, PB, TES, and land costs). Financial parameters are listed in Table 5.

7.4 Results for the Standard Case. As already mentioned all examined solutions shall be equal in terms of annual electricity output. As reference we chose a **PT plant** with the following parameters: **SM = 2, $P_{el,gross}$ = 50 MW, C_{TES} = 8 FLH in Daggett** (all further parameters see Tables 1 and 4) which achieves an annual net energy output W_{net} **of 220 GWh**. All other solutions, which are presented in this study, shall also achieve this energy output. However, the site, SF size, gross electric power, and storage capacity vary.

Figure 10 shows the net aperture area and the gross electrical power for a constant W_{net} of all examined solutions for Daggett.

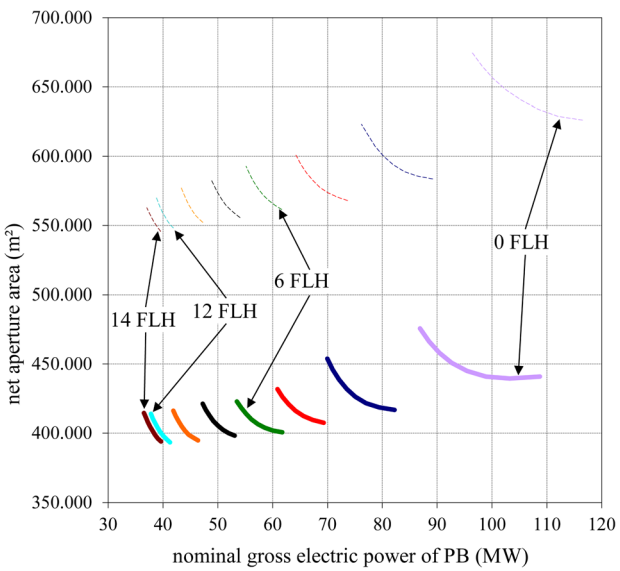

Fig. 10 Plant configurations of PT and LF, W_{net} = 220 GWh, Daggett

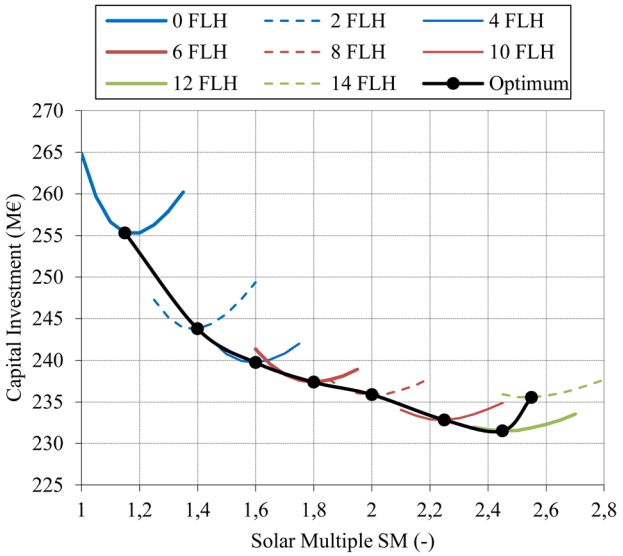

Fig. 11 Solar multiple optimization for the PT system, $W_{net} = 220$ GWh, Daggett

In each category of constant storage capacity constant, W_{net} can be achieved with several combinations of SF size and electrical power of the PB. As expected configurations with a large storage capacity (in FLH) need smaller SFs and smaller PBs to achieve the prescribed electrical yield of 220 GWh. In order to compensate for the inferior optical performance, with the same number of FLH of storage capacity, the LF field must be much larger compared to the PT field. For example, the A_{net} of the LF configurations with 2 FLH exceeds the ones of the PT configurations of about 40%. The nominal electrical power of the PB is also slightly higher for LF systems than for PT systems in each category of storage capacity.

From here, it becomes obvious that the thermodynamic comparison alone is not sufficient, since all presented solutions are technically feasible. In order to proceed, economic figures must be taken into account. Figure 11 shows for each storage capacity the SM with the lowest CI for the PT system. One notices that for each configuration there is a cost-optimum with a specific SM for the PT system. This phenomenon can be explained as follows: By undersizing the SF (low SM) the storage system will be charged less often, and hence, the PB operating hours decrease. By oversizing the SF (high SM) the increase in energy yield saturates and more solar energy must be dumped. Consequently, the increasing costs for the SF are economically not justified. Figure 11 also shows that systems with a storage capacity of 12 FLH achieve the lowest CI. A further increase of storage capacity (e.g., 14 FLH) is not wise, since especially in summer the storage system cannot be discharged anymore during the shorter nights. Hence, the degree of utilization decreases and the CI for the large storage system are economically not justified. However, it should be noted that the result is only valid for constant feed-in-tariff. In an environment, where a special feed-in tariff is paid during bad weather periods a storage capacity with 14 FLH or more could become profitable for the plant's operator.

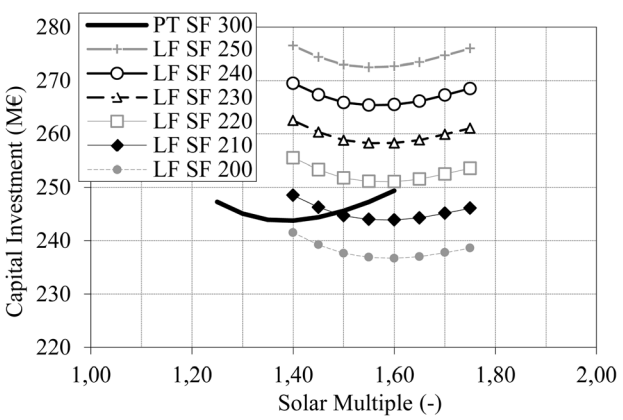

Fig. 12 CI of both systems for 2 FLH, $W_{net} = 220$ GWh, Daggett

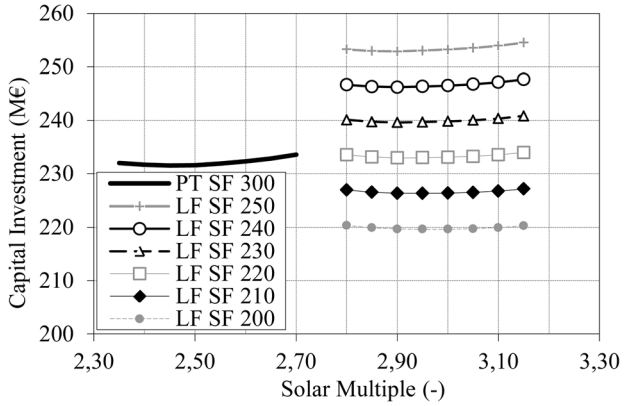

Fig. 13 CI of both systems for 12 FLH, $W_{net} = 220$ GWh, Daggett

Figure 12 shows the CI of all solutions with a storage capacity of 2 FLH, whereas Fig. 13 shows the same with a large storage capacity of 12 FLH. The SF cost of the PT is constant, while for the LF configurations, curves for SF costs between 200 and 250 €/m^2 are shown. With Figs. 12 and 13, the break-even costs of the LF system can be derived, by choosing the LF field costs in the way that the total CI is equal to the CI of the PT system.

Table 6 shows for each category of storage capacity the cost-optimal solution amongst the PT systems with constant W_{net}. The system with the lowest CI is in the category of 12 FLH and is denoted in boldface. Below, the cost-optimal LF solutions are shown, whose CI equals the CI of the PT system in the corresponding category of storage capacity. The area-specific and the relative break-even costs of the SF for these LF solutions are denoted in boldface. Furthermore, the percentage of cofiring that is used for antifreeze COF_{AF} and for direct electricity production COF_{el} is given. It becomes visible that due to lower heat losses the Fresnel system needs a smaller share of the allowed cofiring energy (15% of total thermal energy yield) for antifreeze operation COF_{AF}. The break-even costs LF field in relation to the PT system range from 201.6 €/m^2 at 0 FLH to 221.3 €/m^2 at 14 FLH. Regarding the cost-optimal PT solution (12 FLH), the break-even cost of the corresponding LF field would be 217.8 €/m^2. Apparently, a Fresnel system without TES is especially penalized by the daily course of the optical efficiency (see Sec. 5). With the implementation of a small TES system (2 FLH), this disadvantage is compensated. Generally, it can be concluded, that large storage capacities tend to favor LF systems in this study.

In the following, the same analyzes are carried out for Seville, where also an annual electricity yield of 220 GWh serves as reference. Figure 14 shows the plant layouts of both systems, with constant W_{net} and varying storage capacities. As for Daggett, in Fig. 15 a SM optimization for the PT system is carried out. Figures 16 and 17 show the CI of all solutions for 2 FLH and 12 FLH, respectively. Table 7 shows the cost-optimal PT and LF solutions, as well as the break-even costs of the LF field.

It must be remarked that as for Daggett PT systems with a storage capacity of 12 FLH are the most cost-effective (see Fig. 15). However, the inferior irradiation conditions in Seville move the cost-optimal solution of both system toward higher SM, for example PT with 12 FLH, Daggett: 2.5, PT with 12 FLH, Seville: 2.95 (see Table 7).

Table 6 Cost-optimal configurations for a given storage capacity, W_{net} = 220 GWh, Daggett

Parabolic trough									
C_{TES}	(FLH)	0	2	4	6	8	10	**12**	14
CI	(M€)	255.3	243.8	239.7	237.4	235.9	232.8	**231.5**	235.6
A_{net}	(10^3 m^2)	445.0	426.3	416.2	409.9	405.5	401.7	**398.0**	398.6
COF_{AF}	(%)	43	43	42	42	42	43	**42**	43
COF_{el}	(%)	57	57	58	58	58	57	**58**	57
P_{gross}	(MW)	95.4	75.1	64.2	56.2	50.0	44.0	**40.1**	38.6
SM	(-)	1.15	1.40	1.60	1.80	2.00	2.25	**2.45**	2.55
Linear Fresnel									
C_{TES}	(FLH)	0	2	4	6	8	10	12	14
CI	(M€)	255.3	243.8	239.7	237.4	235.9	232.8	231.5	235.6
A_{net}	(10^3 m^2)	647.7	600.0	582.4	572.0	564.9	560.9	553.2	553.6
COF_{AF}	(%)	12	12	12	12	12	12	12	12
COF_{el}	(%)	88	88	88	88	88	88	88	88
P_{gross}	(MW)	102.6	80.2	67.4	58.3	51.4	45.3	40.8	38.2
SM	(-)	1.35	1.60	1.85	2.10	2.35	2.65	2.90	3.10
$c_{SF,b-e}$	**(€/m^2)**	**201.6**	**209.9**	**213.0**	**214.9**	**216.2**	**215.7**	**217.8**	**221.3**
Rel.	(%)	**67.2**	**70.0**	**71.0**	**71.6**	**72.1**	**71.9**	**72.6**	**73.8**

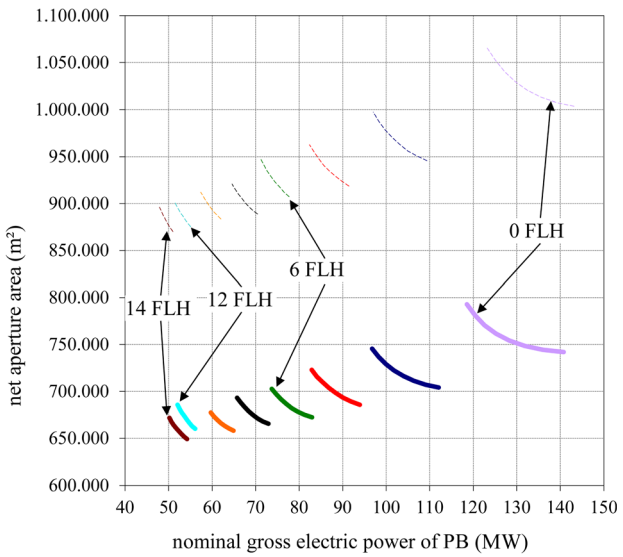

Fig. 14 Plant configurations of PT and LF, W_{net} = 220 GWh, Seville

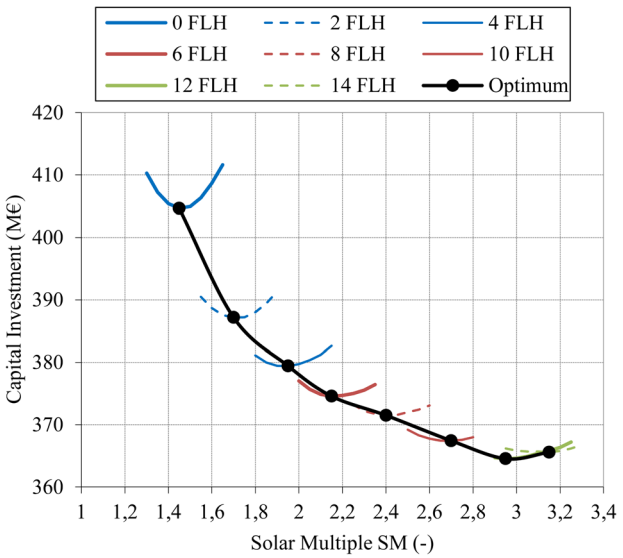

Fig. 15 Solar multiple optimization for the PT system, W_{net} = 220 GWh, Seville

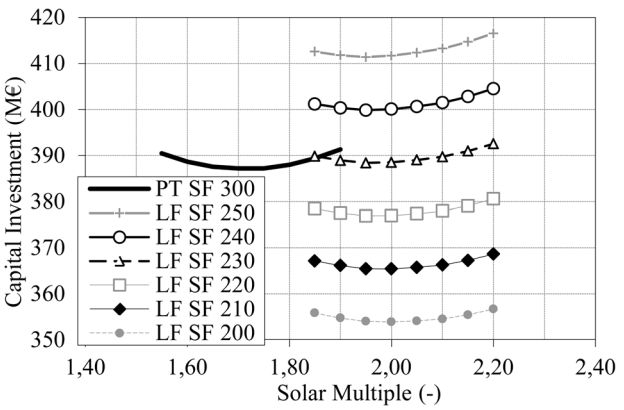

Fig. 16 CI of both systems for 2 FLH, W_{net} = 220 GWh, Seville

Due to inferior meteorological conditions in Seville (see Sec. 4.4), the CI of the PT system increases by 55% to 59% in order to achieve the same W_{net} as in Daggett. Furthermore, the SF is more often in antifreeze mode. This penalizes especially PT systems, which consume about 75% of their allowed cofiring energy directly for antifreeze operation. The LF systems are less affected, since the heat losses of the SF are lower, and therefore, more thermal energy from cofiring can be consumed for electricity production. Hence, the break-even costs of the LF field are higher in Seville: 223.6 for 0 FLH and 234.5 €/m^2 for 12 FLH. In other words, the LF system is favored by the site.

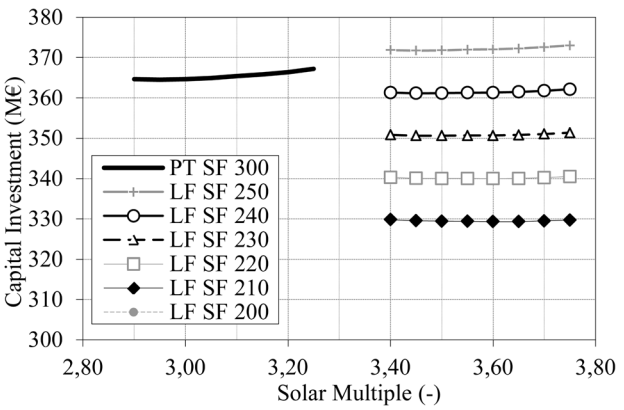

Fig. 17 CI of both systems for 12 FLH, W_{net} = 220 GWh, Seville

Table 7 Cost-optimal configurations for a given storage capacity, W_{net} = 220 GWh, Seville

Parabolic trough									
C_{TES}	(FLH)	0	2	4	6	8	10	**12**	14
CI	(M€)	404.7	387.2	379.4	374.6	371.5	367.4	**364.5**	365.6
A_{net}	(10^3 m^2)	754.3	716.5	698.5	682.4	675.0	669.7	**663.0**	660.7
COF_{AF}	(%)	81	80	79	78	80	79	**79**	79
COF_{el}	(%)	19	20	21	22	20	21	**21**	21
P_{gross}	(MW)	128.3	103.9	88.3	78.3	69.4	61.2	**55.4**	51.7
SM	(-)	1.45	1.70	1.95	2.15	2.4	2.70	**2.95**	3.15
Linear Fresnel									
C_{TES}	(FLH)	0	2	4	6	8	10	12	14
CI	(M€)	404.7	387.2	379.4	374.6	371.5	367.4	364.5	365.5
A_{net}	(10^3 m^2)	1 020.8	956.2	929.2	912.1	896.3	890.6	878.5	873.3
COF_{AF}	(%)	25	24	24	24	24	24	24	24
COF_{el}	(%)	75	76	76	76	76	76	76	76
P_{gross}	(MW)	132.4	104.9	88.4	76.5	68.5	60.5	54.5	50.5
SM	(-)	1.7	2.0	2.3	2.6	2.8	3.2	3.5	3.7
$c_{SF,b-e}$	(€/**m^2**)	**223.6**	**228.9**	**230.6**	**231.6**	**232.2**	**231.7**	**233.2**	**234.5**
Rel.	(%)	**74.5**	**76.3**	**76.9**	**77.2**	**77.4**	**77.2**	**77.7**	**78.2**

Here, it must be mentioned that the advantage for the LF system in Seville occurs in the case of Solar Salt, since the antifreeze temperature in the plant is very high. With another heat transfer fluid, this advantage might not be crucial. Furthermore, the present study does not answer the question of general cost-effectiveness of line-focusing salt systems compared to other systems (such as DSG and synthetic oil).

7.5 Sensitivity of Solar Field Costs. In this section the sensitivity of cost assumptions on the results of Secs. 7–7.4 is examined. In literature, more aggressive costs for PT fields have been published. For example, in Ref. [23], 295 \$/m^2 ∼ 225 €/m^2 as cost target for 2015 is presented. In the same publication, storage costs of 50 \$/kWh$_{th}$ ∼ 38 €/kWh$_{th}$ for 2015 and 25 \$/kWh$_{th}$ ∼ 19 €/kWh$_{th}$ for 2020 are presented as targets. Based on those assumptions, a cost variation for the site Daggett has been carried out. SF costs in the range of 320 €/m^2 down to 200 €/m^2 have been assumed. Additionally, storage costs have been varied from 20 to 50 €/kWh$_{th}$ (30 is the standard case). PB costs are constant.

Figure 18 shows for each category of storage capacity (0–14 FLH) the SM with the minimal CI for a variation of SF costs of the PT system for the site Daggett. The line for SF costs of 300 €/m^2 corresponds to the optimum in Fig. 11. Curves for other cost assumptions are structurally similar on a different magnitude. Again, we find a minimum in CI at about 12 FLH independently from the SF costs (within the presented range of cost variation). With lower SF costs, this minimum slightly moves toward higher SMs since the installation of additional collectors gets cheaper. Based on this set of data, we searched for the corresponding break-even costs of the LF system. In Fig. 19, the evolution of relative break-even costs of the LF system is drawn for the given variation of PT field costs and for each category of storage capacity (0–14 FLH). The *x*-axis shows the relative deviation of PT field costs with 300 €/m^2 as a 100% reference (the reference corresponds to the results of the Sec. 7.4). The diagram shows that the maximum deviation of the relative break-even costs of the LF field is less than one percentage point. From here one could conclude that when PT field costs are reduced, the costs of LF systems must decrease as well, in order to be competitive. However,

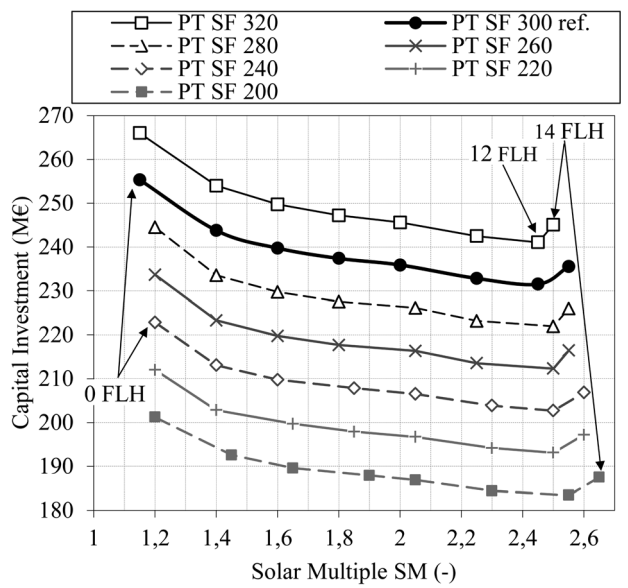

Fig. 18 Cost-optimal SM of a PT plant for each category of storage capacity with SF costs varying from 200 to 320 W/m^2, W_{net} = 220 GWh, Daggett

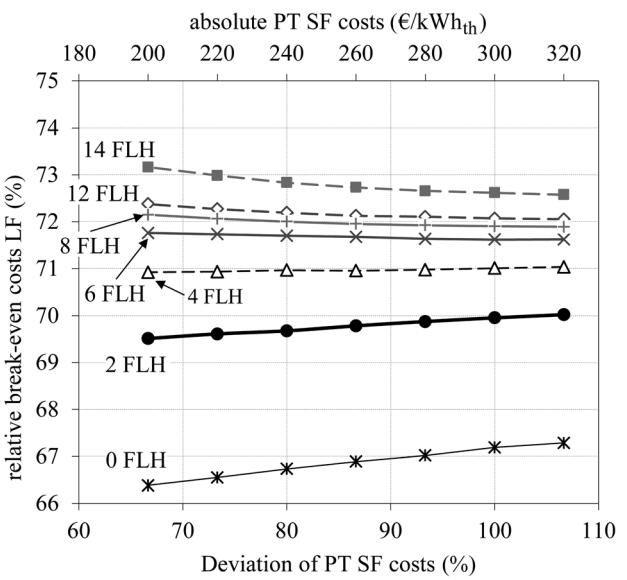

Fig. 19 Sensitivity of cost assumption of PT field on the break-even costs of the LF system, W_{net} = 220 GWh, Daggett

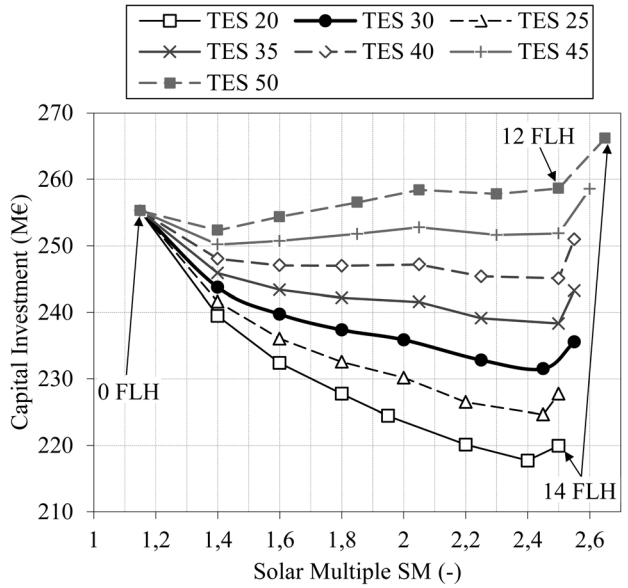

Fig. 20 Cost-optimal SM of a PT plant for each category of storage capacity with storage costs varying from 20 to 50 €/kWh$_{th}$, W_{net} = 220 GWh, Daggett

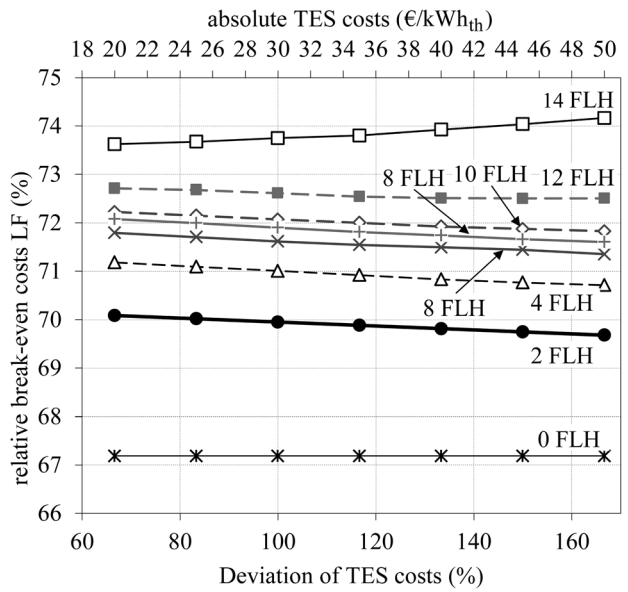

Fig. 21 Sensitivity of cost assumption of TES on the break-even costs of the LF system, W_{net} = 220 GWh, Daggett

the sensitivity of SF field cost on the relative break-even of the LF field is rather marginal.

Similar to Fig. 18, Fig. 20 shows the cost-optimal SM of a PT system for a variation of storage costs from 20 to 50 €/kWh$_{th}$ whereas 30 kWh$_{th}$ represents the reference case. Evidently, the 0 FLH case is the same for each line, since the storage costs are zero. For storage costs up to 40 €/kWh$_{th}$, the plant configuration with a storage capacity of 12 FLH represents the solution with the lowest CI. For storage costs of 45 €/kWh$_{th}$ a cost-optimal system would be found in the category of 2 FLH. A further increase in costs above 50 €/kWh$_{th}$ or more would make the implementation of a storage system unprofitable in general. According to Fig. 19, Fig. 21 shows the sensitivity of the storage costs on the relative break-even costs for each category. Evidently, the line for 0 FLH is horizontal, since there is no storage system. In general, as for the SF cost variation the storage costs only have a rather marginal influence on the relative break-even costs LF fields.

8 Conclusions

In the present publication, in a first step, the optical and the thermodynamic characteristics of a PT and LF field with Solar Salt have been compared. While the optical performance of the LF system cannot match the one of the PT system, heat losses of the Fresnel system are lower due to a smaller number of absorber tubes and a more compact SF. However, the overall thermodynamic performance of the SF is lower.

In a second step, the annual performance of typical PT and LF plant configurations with 0–14 FLH of storage capacity has been compared. The annual electricity yield of various plant configurations has been calculated with a thermodynamic plant model for two sites, Daggett, CA, and Seville, Spain. As boundary conditions the Spanish market with a constant feed-in-tariff and 15% annual cofiring has been chosen. All examined configurations achieve the same net electricity yield of 220 GWh per year.

Results show that a Fresnel system can be implemented in the same thermodynamic process as a PT system and the same annual electricity yield can be attained. In terms of annual yield, the disadvantage of optical performance of the LF system can be compensated by over-sizing the SF. Generally, both systems tend to be more cost-effective with large storage capacities. At both sites, the cost optimum is achieved with a storage capacity of 12 FLH. In order to judge the competitiveness of Fresnel systems, the break-even costs of SF have been calculated. SF costs for the PT system with solar salt of 300 €/m^2 have been assumed. Generally, with large storage capacities break-even costs of the LF field rise; this means that the competitiveness of LF system increases. The break-even costs for Daggett range between 202 €/m^2 (0 FLH) and 221 €/m^2 (14 FLH), or 67–74% of the PT field. For Seville, the break-even cost range between 224 €/m^2 (0 FLH) and 235 €/m^2 (14 FLH), or 75–78%. The site-specific advantage of the LF system is due to the lower heat losses, necessitating less cofiring for antifreeze operation. Nevertheless, it must be noted that this advantage is specific for plants with solar salt and would not necessarily occur with other heat transfer fluids with a significantly lower antifreeze temperature. Eventually, for both sites, the highest break-even costs of the LF field compared to the PT field are achieved with large storage capacities.

In order to confirm the major statements of the present paper, the costs of the PT field have been varied from 200 €/m^2 to 320 €/m^2 and the storage costs have been varied from 20 €/kWh$_{th}$ to 50 €/kWh$_{th}$ for the site Daggett. Results show that within the given variation of cost structure the relative break-even costs for LF systems do not significantly change.

Nomenclature

DSG = direct steam generation
LF = linear Fresnel
PB = power block
PT = parabolic trough
SF = solar field
SM = solar multiple
TES = thermal energy storage

Symbols

A = aperture area of solar field (m^2)
c = area-specific costs (€/m^2)
C = thermal capacity (h)
CI = capital investment costs (M€)
COF = fraction of cofiring (%)
DNI = direct normal irradiance (W/m^2)
FLH = full load hours (h)
IAM = incident angle modifier

P = electrical power (MW)
$\dot{q}$ = area-specific power (W/m^2)
Q = thermal power (MW)
T = temperature (°C)
W_{net} = produced electricity (MW h)
α = elevation angle (deg)
η = efficiency
ρ = angle (tracking of PT) (deg)
θ = angle (incidence or transversal for LF) (deg)

Subscripts

amb = ambient
AF = antifreeze
b-e = break even
clean = cleanliness
col = collector
el = electricity
end = end of collector
gross = gross (e.g., in gross el. power)
H&P = header and piping
i = incidence
loss = heat losses
net = net aperture/net electricity
nom = nominal
opt = optical
s = sun
shad = shading
solar = solar
therm = thermal
tr = tracking
trans = transversal

References

[1] Dersch, J., Morin, G., Eck, M., and Häberle, A., 2009, "Comparison of Linear Fresnel and Parabolic Trough Collector Systems—System Analysis to Determine Break-Even Costs of Linear Fresnel Collectors," Proceedings of the 15th International SolarPACES Symposium, Berlin Germany, Sept. 15–18.

[2] Giostri, A., Binotti, M., Silva, P., Macchi, E., and Manzolini, G., 2011, "Comparison of Two Linear Collectors in Solar Thermal Plants: Parabolic Trough vs. Fresnel," ASME Paper No. ES2011-54312.

[3] Morin, G., Dersch, J., Platzer, W., Eck, M., and Häberle, A., 2012, "Comparison of Linear Fresnel and Parabolic Trough Collector Power Plants," Sol. Energy, **86**(1), pp. 1–12.

[4] Winter, C. J., Sizmann, R. L., and Vant-Hull, L. L., 1991, *Solar Power Plants: Fundamentals, Technology, Systems, Economics*, 1st ed., Springer, Berlin/Heidelberg, Germany.

[5] Solarlite, 2011, "Press Release: TSE 1—The First Parabolic Trough Plant Using Direct Steam Generation—Delivers Its Full 5 MW of Output to Thailand's Power Network," Duckwitz, Jan. 26, 2011.

[6] Eck, M., Eickhoff, M., Feldhoff, J. F., Fontela, P., Gathmann, N., Meyer-Grünefeldt, M., Hillebrand, S., and Schulte-Fischedick, J., 2011, "Direct Steam Generation in Parabolic Troughs at 500 °C—First Results of the REAL-DISS Project," Proceedings of the 17th SolarPACES Conference, Granada, Spain, Sep. 20–23.

[7] Selig, M., and Mertins, M., 2010, "From Saturated to Superheated Direct Solar Steam Generation—Technical Challenges and Economical Benefits," Proceedings of the 16th SolarPaces Conference, Perpignon, France, Sep. 21–24, p. 8.

[8] Novatec Solar, 2011, "Press Release: Novatec Solar's Fresnel Collector Generates Superheated Steam Above 500 °C," Karlsruhe, Sept. 22, 2011.

[9] Riffelmann, K.-J., Graf, D., and Nava, P., 2011, "Ultimate Trough—The New Parabolic Trough Collector Generation for Large Scale Solar Thermal Power Plants," ASME Paper No. ES2011-54657.

[10] Fernández-García, A., Zarza, E., Valenzuela, L., and Pérez, M., 2010, "Parabolic-Trough Solar Collectors and Their Applications," Renewable Sustainable Energy Rev., **14**(7), pp. 1695–1721.

[11] Lüpfert, E., 2005, "PARFOR—Testreport PTR Parabolic Trough Receiver 2005—Modelling Parameters from Test Results," Technical Report DLR, Cologne, Germany.

[12] Burkholder, F., and Kutscher, C., 2009, "Heat Loss Testing of Schott's 2008 PTR70 Parabolic Trough Receiver," National Renewable Energy Laboratory, Technical Report No. NREL/TP-550–45633.

[13] Schott Solar, 2011, *Schott PTR 70 Receiver—Setting the Benchmark*, Mainz, Germany.

[14] Conlon, W. M., 2011, "Direct Steam From CLFR Solar Steam Generators," Proceedings of the 17th SolarPACES Conferences, Granada, Spain, Sept. 20–23.

[15] Eck, M., Bernhard, R., De Lalaing, J., Kistner, R., Eickhoff, M., Feldhoff, J. F., Heimsath, A., Hülsey, H., and Morin, G., 2009, "Linear Fresnel Collector Demonstration at the PSA—Operation and Investigation," Proceedings of the 15th CSP SolarPACES Symposium, R. Pitz-Paal, ed., Berlin, Germany, Sept. 15–18.

[16] Novatec Solar, 2011, "Press Release: Novatec Solar's Fresnel collector generates superheated steam above 500 °C," Karlsruhe, Germany, Sept. 11, 2011.

[17] NREL, 2012, "Renewable Resource Data Center." Available at: http://www.nrel.gov/rredc/

[18] Meteotest, 2012, "Irradiational Data for Every Place of Earth." Available at: http://meteonorm.com

[19] Kearney, D., Herrmann, U., Nava, P., Kelly, B., Mahoney, R., Pacheco, J., Cable, R., Potrovitza, N., Blake, D., and Price, H., 2003, "Assessment of a Molten Salt Heat Transfer Fluid in a Parabolic Trough Solar Field," ASME J. Sol. Energy Eng., **125**(2), pp. 170–176.

[20] Solar Millennium, 2009, "The Parabolic Trough Power Plants Andasol 1 to 3—The Largest Solar Power Plants in the World—Technology Premiere in Europe," Sept. 22, 2011, Solar Millennium, Erlangen Germany.

[21] Kolb, G., 2011, "An Evaluation of Possible Next-Generation High-Temperature Molten-Salt Power Towers," Sandia National Laboratories, Albuquerque, NM, Technical Report No. SAND2011-9320.

[22] Pitz-Paal, R., Dersch, J., and Milow, B., 2003, "Ecostar—European Concentrated Solar Thermal Road-Mapping," DLR, Technical Report No. SES6-CT-2003-502578.

[23] Turchi, C., Mehos, M., Ho, C. K., and Kolb, G. J., 2010, "Current and Future Costs for Parabolic Trough and Power Tower Systems in the US Market," Proceedings of the 16th SolarPACES Conference, Perpignan, France.